A stochastic averaging mathematical framework for design and optimization of nonlinear energy harvesters with several electrical DOFs

Commun Nonlinear Sci Numer Simulat 139 (2024) 108306

Contents lists available at ScienceDirect

Communications in Nonlinear Science and Numerical Simulation

journal homepage: www.elsevier.com/locate/cnsns

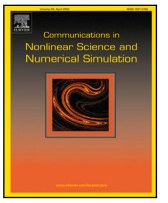

Research paper

A stochastic averaging mathematical framework for design and optimization of nonlinear energy harvesters with several electrical DOFs

Kailing Song [a,b], Michele Bonnin [b,*], Fabio L. Traversa [c], Fabrizio Bonani [b]

[a] IUSS, University School for Advanced Studies, Pavia, 27100, Italy
[b] Department of Electronics and Telecommunications, Politecnico di Torino, Torino, 10129, Italy
[c] Memcomputing Inc., San Diego, 92121, CA, United States

ARTICLE INFO

Keywords:
Energy harvesting
Mechanical vibrations
Electro-mechanical systems
Nonlinear dynamical systems
Model order reduction
Stochastic processes
Stochastic differential equations
Stochastic averaging
Fokker–Planck equation
Impedance matching

ABSTRACT

Energy harvesters for mechanical vibrations are electro-mechanical systems designed to capture ambient dispersed kinetic energy, and to convert it into usable electrical power. The random nature of mechanical vibrations, combined with the intrinsic non-linearity of the harvester, implies that long, time domain Monte-Carlo simulations are required to assess the device performance, making the analysis burdensome when a large parameter space must be explored. Therefore a simplified, albeit approximate, semi-analytical analysis technique is of paramount importance. In this work we present a methodology for the analysis and design of nonlinear piezoelectric energy harvesters for random mechanical vibrations. The methodology is based on the combined application of model order reduction, to project the dynamics onto a lower dimensional space, and of stochastic averaging, to calculate the stationary probability density function of the reduced variables. The probability distribution is used to calculate expectations of the most relevant quantities, like output voltage, harvested power and power efficiency. Based on our previous works, we consider an energy harvester with a matching network, interposed between the harvester and the load, that reduces the impedance mismatch between the two stages. The methodology is applied to the optimization of the matching network, allowing to maximize the global harvested power and the conversion efficiency. We show that the proposed methodology gives accurate predictions of the harvester's performance, and that it can be used to significantly simplify the analysis, design and optimization of the device.

1. Introduction

The importance of energy harvesting for the implementation of sustainable, smart applications that require energy-efficient electronic devices and sensors, e.g. the Internet of Things (IoT), can hardly be overestimated [1,2]. In most cases, IoT elements exchange information by exploiting wireless technologies, an operational paradigm that of course requires the availability of an electrical energy source. Dedicated design and the relatively small distance between elements granted by the large number of nodes allow for reduction of the required power to levels low enough to make energy extraction from ambient dispersed sources a viable solution [3,4].

Depending on the intended application, different energy sources can be used, including parasitic mechanical vibrations, electromagnetic dispersed energy, thermal gradients, and even human motion [5–7]. Ambient vibrations are especially promising

* Corresponding author.
E-mail address: michele.bonnin@polito.it (M. Bonnin).

https://doi.org/10.1016/j.cnsns.2024.108306
Received 12 March 2024; Received in revised form 2 July 2024; Accepted 21 August 2024
Available online 30 August 2024

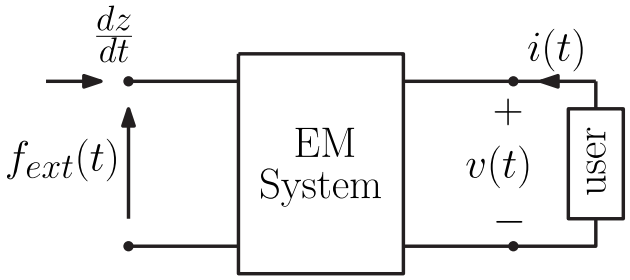

Fig. 1. Two-port network representation of a energy harvester for mechanical vibrations.

for their ubiquity, significant power density, and the wide range of transduction principles available for energy conversion [8,9]. In particular, Si-based mechanical structures covered by a piezoelectric material providing energy transduction, are one of the most studied examples of energy harvesters, due to their compatibility with well-established semiconductor technologies [10].

Despite significant research efforts, the harvested power provided to the electrical load remains confined to the micro-to-milli-Watt range, thus requiring further optimization efforts to boost the performance [11–13]. A key limiting factor is the frequency mismatch between environmental vibrations, the mechanical structure of the harvester, and the electrical domain. As a rule of thumb, the resonance frequency of a mechanical structure is inversely proportional to its geometrical dimensions. The typical size of mechanical resonators (in the range from millimeters to centimeters) implies that they exhibit optimal performance at hundreds, or thousands of Hertz, while electrical circuits typically exhibit a resonance frequency at kilo Hertz or above. In contrast, ambient vibrations have considerable energy density over frequencies within 100 Hertz [14–17].

A possible solution to increase the harvested power is to use nonlinear resonators instead of linear ones. Nonlinear systems serve dual purposes: they offer larger bandwidth (at the cost of less peak power), and they may exhibit multi-stability, enhancing the response of the system by increasing oscillation amplitude [18–26]. Recently, new solutions inspired by circuit theory have been proposed. The first solution consists of connecting an inductor in parallel to the load, to compensate for the negative reactance of the piezoelectric transducer [27–29]. The more sophisticated solution is to interpose a more complex matching network between the transducer and the load [30,31]. Semi-active control techniques have also been developed and tested [32–34].

As the number of structures and components in the harvester increases, the corresponding mathematical model grows in complexity, making analysis, design, and optimization more challenging. The problem is exacerbated by the nonlinear nature of the system, and by the stochastic nature of mechanical vibrations. To cope with the problem, in this paper we present a novel methodology for the effective analysis and optimization of nonlinear piezoelectric energy harvesters subject to stochastic external forces. We combine a model order reduction technique, to reduce the model complexity to a single variable description (the mechanical energy in the device), with stochastic averaging, to allow for the computation of the stationary probability density function of the reduced model. The probability density function is then used to estimate the expected quantities in the harvester, including the power delivered to the electrical load for both a simple resistive element and for the matching network, enabling an improved electrical power transfer to the load.

The methodology permits a semi-analytical calculation of the harvested power and output voltage, making it relatively easy to exploit a large parameter space for the matching network optimization. In contrast, standard approaches, based on Monte-Carlo simulations, would require intensive computation and lengthy simulations, making the approach unfeasible, or at least unpractical, for systems characterized by a larger number of parameters.

The paper structure is as follows: the model of the nonlinear harvester is described in Section 2. The novel methodology is presented in Section 3, where the approximating theory is developed by combining the model order reduction approach with stochastic averaging. Examples of applications are presented for both a resistive and the matched load in Section 4, validating the proposed methodology against a Monte Carlo solution of the complete, nonlinear model. Finally, conclusions are drawn in Section 5.

2. Nonlinear system modeling

Energy harvesters for ambient mechanical vibrations are electro-mechanical (EM) systems, which can be represented as the two-port network shown in Fig. 1. Mechanical quantities like force and velocity are applied at the left port, whereas electrical variables like current and voltage are applied at the right port. In this representation, the passive sign convention is used for the two-port network. Finally, a two-terminal element is connected at the output terminals, representing a generic user device that absorbs electrical power or receives information from the EM network.

Irrespective of the working principle, the internal structure of an energy harvester for ambient vibrations always requires an oscillating element to capture the environmental kinetic energy. Different transduction principles are available for mechanical-to-electrical energy conversion, such as the piezoelectric effect, electromagnetic induction, or electrostatic (capacitive) conversion. Many different designs and ingenious solutions have been proposed for piezoelectric energy harvesters, aimed at increasing the

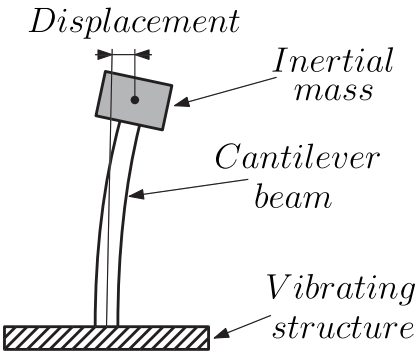

Fig. 2. Schematic representation of a cantilever beam, piezoelectric energy harvester for ambient mechanical vibrations.

power performance and efficiency. Recent comprehensive reviews on the state-of-the-art of piezoelectric energy harvesting can be found in [35,36].

We consider here a cantilever beam-based, piezoelectric energy harvester, whose schematic representation is shown in Fig. 2. The oscillating structure is represented by the cantilever beam, which is fixed at one end to a vibrating structure. Vibrations of the support induce oscillations of the beam, which are amplified by an inertial mass fixed at the cantilever free end, and finally are converted into electrical power by a layer of piezoelectric material that covers the beam. The beam is assumed to have a rectangular cross-section, so that oscillations are forced to occur along one dimension, and the oscillation amplitude is assumed to be so small with respect to the beam length, that the arc-shaped displacement can be approximated by a straight line.

Assuming that the masses of the beam and piezoelectric layer are negligible with respect to the inertial mass (denoted as m), we have the Lagrangian function $\mathcal{L}(z,\dot{z}) = T(\dot{z}) - \hat{U}(z) = (1/2)m\,\dot{z}^2 - \hat{U}(z)$, where z, $\dot{z}$ are the displacement and the velocity, respectively. Consequently, $T(\dot{z})$, $\hat{U}(z)$ are the kinetic and the potential energy functions. Introducing also the dissipation potential $D(\dot{z}) = (1/2)\hat{\varepsilon}\,\dot{z}^2$, where $\hat{\varepsilon}$ is the friction coefficient, the Lagrange equation of motion for the mechanical system takes the form

$$m\ddot{z} + \hat{\varepsilon}\dot{z} + \hat{U}'(z) = f_{ext}(t) - f_{el}(\mathbf{z}_e) \tag{1}$$

where $f_{ext}(t)$ is an external force representing mechanical vibrations, and $f_{el}(\mathbf{z}_e)$ is a mechanical force due to the action of the electrical variables $\mathbf{z}_e$. For the sake of simplicity, we shall assume that the resultant force has the same order of magnitude as the internal friction and that $f_{el}(\mathbf{z}_e)$ is linear and of the form $f_{el}(\mathbf{z}_e) = \hat{\varepsilon}\,\hat{\mathbf{b}}_m^T\,\mathbf{z}_e$, where $\hat{\mathbf{b}}_m = [b_{m1},\dots,b_{mn}]^T$ is a vector of electro-mechanical coupling constants, and ^{T} denotes transposition.

The electrical domain is described by a linear circuit, composed of the interconnection of linear two-terminal (or multi-terminal) elements. Consequently, the state equations are a linear system of ordinary differential equations (ODEs), which can be derived using Kirchhoff voltage and current laws, and the characteristic relationships of the electrical elements [37], thereby obtaining the ODEs system:

$$\dot{\mathbf{z}}_e = \hat{\mathbf{A}}_e\mathbf{z}_e + \hat{\mathbf{B}}_e\,\mathbf{z}_m \tag{2}$$

where $\mathbf{z}_e : \mathbb{R} \mapsto \mathbb{R}^n$ is the vector of electrical state variables (currents through inductors and voltages across capacitors), $\hat{\mathbf{A}}_e \in \mathbb{R}^{n,n}$ and $\hat{\mathbf{B}}_e \in \mathbb{R}^{n,2}$ are real valued matrices, and $\mathbf{z}_m = [z,\dot{z}]^T$ is the vector of mechanical variables.

Finally, we consider the modeling of vibrations. Being the byproduct of the ambient conditions influencing the harvester, such vibrations are the superposition of several distinct, and most often independent, sources of different nature and various time dependencies. Examples of vibration sources are household appliance, industrial machinery, human motion, vehicles such as automobiles, trains and airplanes and structures such as buildings and bridges. Vibrations frequency may range from few Hz (human motion), to some hundreds of Hz (for domestic and industrial machinery), up to some kHz (acoustic waves). As the number of sources grows large, the central limit theorem suggests that vibrations become Gaussian distributed, and in case the corresponding energy is distributed over a sufficiently wide frequency spectrum, random vibrations can ultimately be well approximated as white Gaussian noise [18,26,28,38].

Under the above assumptions, (1) and (2) can be rewritten as a system of stochastic differential equations (SDEs):

$$dZ_1 = Z_2\,dt \tag{3a}$$

$$dZ_2 = \left(-\frac{1}{m}\hat{U}'(Z_1) - \frac{\hat{\varepsilon}}{m}Z_2 + \frac{\hat{\varepsilon}}{m}\hat{\mathbf{b}}_m^T\mathbf{Z}_e\right)dt + \frac{\sqrt{\hat{\varepsilon}}}{m}dW_t \tag{3b}$$

$$d\mathbf{Z}_e = \left(\hat{\mathbf{A}}_e\mathbf{Z}_e + \hat{\mathbf{B}}_e\mathbf{Z}_m\right)dt \tag{3c}$$

where $Z_1 = z$ is the displacement and $Z_2 = \dot{z}$ is the velocity. Hereinafter we adopt the standard notation used in probability: A capital letter denotes a random variable, while a lowercase letter denotes its possible value. In Eq. (3), W_t is a scalar Wiener process, also known as Brownian motion, it is the integral of a white Gaussian process and it is characterized by a zero expectation ($\mathrm{E}[W_t] = 0$,

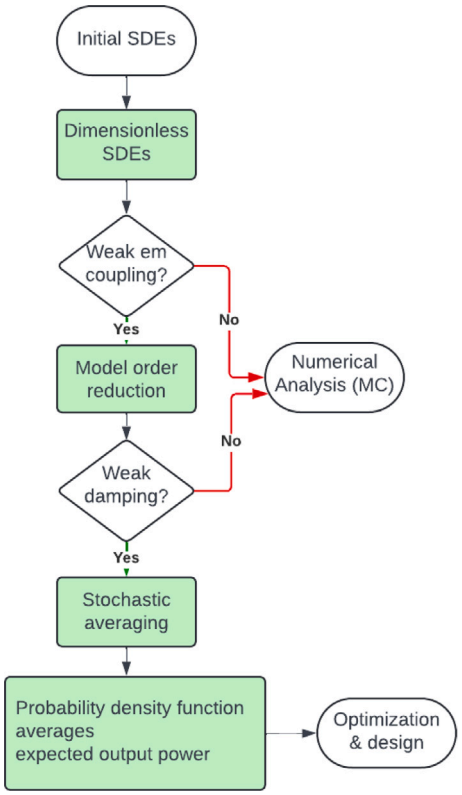

Fig. 3. Schematic flowchart of the proposed methodology for the analysis and design of an energy harvesting system for random mechanical vibrations.

where E[·] represents the statistical average) and covariance $\mathrm{cov}(W_t, W_s) = \mathrm{E}[W_t\, W_s] = \min(t, s)$. In other words, $W_t \sim \mathcal{N}(0, t)$ where symbol $\sim$ means "distributed as", and $\mathcal{N}(0, t)$ denotes the centered normal distribution.

The SDEs (3) can be interpreted following two main rules: Stratonovich or Itô [39]. Because the noise in (3) is unmodulated (or additive), the two interpretations lead to the same results, although the calculus rules used in the derivation are different. In the following, we shall use Itô interpretation for all SDEs.

3. Model reduction and stochastic averaging

In this section, we present the methodology for the analysis of energy harvesting systems, which main steps are summarized in Fig. 3. The derivation of the dimensionless SDEs is based on a systematic procedure, that is described in details in [26,40]. Examples of transformation to dimensionless equations are given in Section 4, in Eqs. (25)–(28) and (37)–(39). The subsequent steps are based on the application of a model order reduction technique, followed by stochastic averaging. The applicability of both techniques requires some technical conditions to hold, in particular a small electro-mechanical coupling between the electrical and the mechanical domains, and a weak mechanical damping. Both conditions are usually well met in energy harvesting applications.

The nonlinear SDE system (3) can be cast in the form

$$d\mathbf{Z}_t = \left(\hat{\mathbf{A}}\mathbf{Z}_t + \hat{\mathbf{n}}(\mathbf{Z}_t)\right) dt + \hat{\mathbf{B}}\, dW_t \tag{4}$$

where $\mathbf{Z}_t = [Z_1, Z_2, \mathbf{Z}_e^T]^T$ is the state vector, $\hat{\mathbf{A}}\mathbf{Z}_t$ and $\hat{\mathbf{n}}(\mathbf{Z}_t)$ are the linear and the nonlinear parts of the drift vector, respectively, and $\hat{\mathbf{B}}$ is the (constant) diffusion vector. In order to simplify the treatment, we transform (3) in a scaled, dimensionless equivalent SDE system. Consider a linear change of variables $\mathbf{x} = \mathbf{P}\mathbf{z}$, where $\mathbf{P}$ is a regular matrix, and a linear time change $\tau = \omega t$, with $\omega > 0$. Let $\mathbf{A} = (1/\omega)\mathbf{P}\hat{\mathbf{A}}\mathbf{P}^{-1}$, $\mathbf{n}(\mathbf{x}) = (1/\omega)\mathbf{P}\hat{\mathbf{n}}(\mathbf{P}^{-1}\mathbf{x})$ and $\mathbf{B} = (1/\sqrt{\omega})\mathbf{P}\hat{\mathbf{B}}$. Then the solution of the SDE system

$$d\mathbf{X}_\tau = \left(\mathbf{A}\,\mathbf{X}_\tau + \mathbf{n}(\mathbf{X}_\tau)\right) d\tau + \mathbf{B}\, dW_\tau \tag{5}$$

converges in probability to $\mathbf{P}\mathbf{Z}_t$.

Convergence in probability, or weak convergence, implies that the two stochastic processes have the same probability distribution, and therefore the same statistical properties. Thus, introducing a proper diagonal matrix $\mathbf{P}$ whose entries are normalizing

factors, and a normalizing frequency ω, the following SDE system equivalent to (3) is obtained, for the dimensionless process[1] $\mathbf{X}_t$:

$$dX_1 = X_2\, dt \tag{6a}$$

$$dX_2 = \left(-U'(X_1) - \varepsilon X_2 + \varepsilon\, \mathbf{b}_m^T \mathbf{X}_e\right) dt + \sqrt{\varepsilon}\, B_m\, dW_t \tag{6b}$$

$$d\mathbf{X}_e = \left(\mathbf{A}_e \mathbf{X}_e + \mathbf{b}_1 X_1 + \mathbf{b}_2 X_2\right) dt \tag{6c}$$

Here $\mathbf{X}_t = [X_1, X_2, \mathbf{X}_e^T]^T$ is the vector of the dimensionless state variables (mechanical and electrical), ε is a dimensionless parameter, $\mathbf{b}_1 \in \mathbb{R}^n$ and $\mathbf{b}_2 \in \mathbb{R}^n$ are the columns of a dimensionless matrix $\mathbf{B}_e \in \mathbb{R}^{n,2}$.

3.1. Model order reduction

The concept of model order reduction refers to a set of methods aimed at simplifying a complex mathematical model, for example reducing the number of state variables, while preserving the model's essential characteristic [41]. In this work, we apply a method similar to that used in [40,42], to reduce the number of variables in (6) by exploiting the time scale separation between mechanical and electrical variables, so that the latter can be eliminated.

Consider the dimensionless mechanical energy: $E = (1/2)X_2^2 + U(X_1)$. Application of Itô formula gives

$$dE = \varepsilon \left(\frac{B_m^2}{2} - X_2^2 + \mathbf{b}_m^T \mathbf{X}_e \right) dt + \sqrt{\varepsilon} B_m X_2\, dW_t \tag{7}$$

As a consequence, for $\varepsilon \ll 1$, the mechanical energy is a slow, or nearly constant, variable (see [40] for details). Following [42], we assume $X_1(t) = A(E)\sin(\Omega(E)t)$, where $A(E)$ and $\Omega(E)$ are an unknown amplitude and angular frequency, respectively. Because the energy is nearly constant, (6a) implies $X_2(t) \simeq \Omega(E)A(E)\cos(\Omega(E)t)$.

At this point, we look for a solution to (6c) in the form

$$\mathbf{X}_e = \mathbf{m}_1(E)X_1 + \mathbf{m}_2(E)X_2 \tag{8}$$

where, considering that E is nearly constant, $\mathbf{m}_1(E)$, and $\mathbf{m}_2(E)$ are unknown, constant vectors.

Since the differential equation for the electrical domain (6c) is linear, vectors $\mathbf{m}_1(E)$ and $\mathbf{m}_2(E)$ can be computed analytically.

Lemma 1. *Under the above assumptions on $X_1(t)$ and $X_2(t)$, vectors $\mathbf{m}_1(E)$ and $\mathbf{m}_2(E)$ are given by*

$$\mathbf{m}_1(E) = -\mathbf{A}_e \left(\mathbf{A}_e^2 + \Omega^2(E)\mathbb{1}\right)^{-1} (\mathbf{A}_e \mathbf{b}_2 + \mathbf{b}_1) + \mathbf{b}_2 \tag{9a}$$

$$\mathbf{m}_2(E) = -\left(\mathbf{A}_e^2 + \Omega^2(E)\mathbb{1}\right)^{-1} (\mathbf{A}_e \mathbf{b}_2 + \mathbf{b}_1) \tag{9b}$$

where $\mathbb{1} \in \mathbb{R}^{n,n}$ is the $n \times n$ identity matrix.

Proof. The assumed value of $X_1(t)$ and $X_2(t)$ imply, in the frequency domain, the following phasor representations

$$X_1 \to A(E) \tag{10a}$$

$$X_2 \to j\Omega(E)A(E) \tag{10b}$$

$$\mathbf{X}_e \to \left(\mathbf{m}_1(E) + j\Omega(E)\,\mathbf{m}_2(E)\right) A(E) \tag{10c}$$

$$\frac{d\mathbf{X}_e}{dt} \to \left(j\Omega(E)\mathbf{m}_1(E) - \Omega^2(E)\mathbf{m}_2(E)\right) A(E) \tag{10d}$$

Substituting into Eq. (6c), and equating the real and imaginary parts, the thesis follows. □

Lemma 2. *For every stable circuit, matrix $\left(\mathbf{A}_e^2 + \Omega^2(E)\mathbb{1}\right)$ is invertible.*

Proof. Let λ_i, be an eigenvalue of $\mathbf{A}_e$ and let $\mathbf{v}_i$ be the corresponding eigenvector. Then:

$$\mathbf{A}_e^2\, \mathbf{v}_i = \mathbf{A}_e(\mathbf{A}_e \mathbf{v}_i) = \lambda_i \mathbf{A}_e\, \mathbf{v}_i = \lambda_i^2 \mathbf{v}_i$$

$$\Omega^2 \mathbb{1}\mathbf{v}_i = \Omega^2 \mathbf{v}_i$$

that is, $\mathbf{v}_i$ is an eigenvector of $(\mathbf{A}_e^2 + \Omega^2(E)\mathbb{1})$ associated to the eigenvalue $\lambda_i^2 + \Omega^2(E)$. For a stable linear circuit $\mathrm{Re}\{\lambda_i\} < 0$, for all $i = 1, \ldots, n$. If $\lambda_i \in \mathbb{R}$, then $\lambda_i^2 + \Omega^2(E)$ is real and positive, for all $i = 1, \ldots, n$. Conversely, if $\lambda_i \in \mathbb{C}$, then $\mathrm{Im}\{\lambda_i^2 + \Omega^2(E)\} = 2\mathrm{Re}\{\lambda_i\}\mathrm{Im}\{\lambda_i\} \neq 0$. Thus zero is not an eigenvalue of $(\mathbf{A}_e^2 + \Omega^2(E)\mathbb{1})$ and the matrix is invertible. □

The reduced order model is obtained substituting (8) into (6b)

$$dX_1 = X_2\, dt \tag{11a}$$

$$dX_2 = \left(-U'(X_1) + \varepsilon\, \mathbf{b}_m^T \mathbf{m}_1(E)X_1 + \varepsilon(\mathbf{b}_m^T \mathbf{m}_2(E) - 1)X_2\right)dt + \sqrt{\varepsilon} B_m\, dW_t \tag{11b}$$

[1] For the sake of simplicity, we have used the same symbol t also for the normalized time.

3.2. Stochastic averaging

The second step in the derivation of a reduced model amounts in rewriting the SDE system in terms of new variables: the dimensionless mechanical energy and a mechanical angle, and then removing the latter through stochastic averaging.

For $\varepsilon = 0$, system (11) describes a Hamiltonian system, having $E = (1/2)X_2^2 + U(X_1)$ as a first integral. Hamiltonian systems can be rewritten in terms of the energy and an angle coordinates, such that the state equations take the form [43]:

$$\frac{dE}{dt} = 0 \tag{12a}$$

$$\frac{d\theta}{dt} = \Omega(E) \tag{12b}$$

where θ is the angle function and $\Omega(E)$ is the angular frequency.

For small values of ε, the implicit function theorem guarantees that the coordinate transformation $(X_1, X_2) \to (E, \theta)$ is locally invertible. This implies that, within the limits of small values for ε, we can derive the SDE system for the energy and angle variables.

Theorem 1 (*Energy-angle SDEs*)**.** *Consider the SDE system* (11) *and assume that an explicit expression for the angle variable as a function of the original coordinates is available in the form* $\theta = \theta(X_1, X_2)$*, then the energy and the angle are solutions of the SDE system*

$$dE = \varepsilon a_E(E,\theta)dt + \sqrt{\varepsilon} B_E(E,\theta)dW_t \tag{13a}$$

$$d\theta = \big(\Omega(E) + \varepsilon a_\theta(E,\theta)\big)dt + \sqrt{\varepsilon} B_\theta(E,\theta)dW_t \tag{13b}$$

where (explicit dependence on E *and* θ *is dropped in* $X_1(E,\theta)$*,* $X_2(E,\theta)$*, for simplicity of notation)*

$$a_E(E,\theta) = \frac{1}{2}B_m^2 + X_2\, f(X_1, X_2) \tag{14a}$$

$$B_E(E,\theta) = B_m\, X_2 \tag{14b}$$

$$\Omega(E) = \frac{\partial\theta}{\partial X_1} X_2 - \frac{\partial\theta}{\partial X_2} U'(X_1) \tag{14c}$$

$$a_\theta(E,\theta) = \frac{\partial\theta}{\partial X_2} f(X_1, X_2) + \frac{1}{2}\frac{\partial^2\theta}{\partial X_2^2} B_m^2 \tag{14d}$$

$$B_\theta(E,\theta) = \frac{\partial\theta}{\partial X_2}\, B_m \tag{14e}$$

being

$$f(X_1, X_2) = \mathbf{b}_m^T \mathbf{m}_1(E) X_1 + (\mathbf{b}_m^T \mathbf{m}_2(E) - 1) X_2 \tag{14f}$$

Proof. The proof is a straightforward application of Itô formula, using the definition of the dimensionless energy and angle variables, and observing that, for the unperturbed system, (12b) implies (14c). □

After deriving the governing equations in the energy-angle representation (13), we aim at eliminating the angle variable. According to Khasminskii's stochastic averaging theorem [44], the slow varying process E converges in probability as $\varepsilon \to 0$ to a one dimensional Markov process, in a time interval $[0, T]$ with $T = \mathcal{O}(1/\varepsilon)$. The Itô SDE for the one dimensional Markov process is obtained by averaging the original SDE (13a) with respect to the fast variable, while the slow one is kept constant [44,45], thereby obtaining

$$dE \simeq \varepsilon \overline{a}_E(E)dt + \sqrt{\varepsilon}\, \overline{B}_E(E)dW_t \tag{15}$$

where the averaged coefficients are

$$\overline{a}_E(E) = \lim_{T\to+\infty} \frac{1}{T} \int_0^T a_E(E, \theta(t))\, dt \tag{16a}$$

$$\overline{B}_E(E) = \sqrt{\lim_{T\to+\infty} \frac{1}{T} \int_0^T B_E^2(E, \theta(t))\, dt} \tag{16b}$$

and $\theta(t)$ is the solution of the fast equation, calculated while keeping the slow variable E constant. For $\varepsilon \to 0$, the fast equation admits the solution $\theta = \Omega(E)t + \theta_0$, where θ_0 is an arbitrary initial condition, and the averaged coefficients become

$$\overline{a}_E(E) = \frac{1}{2\pi} \int_0^{2\pi} a_E(E, \theta)\, d\theta \tag{17a}$$

$$\overline{B}_E(E) = \sqrt{\frac{1}{2\pi} \int_0^{2\pi} B_E^2(E, \theta)\, d\theta} \tag{17b}$$

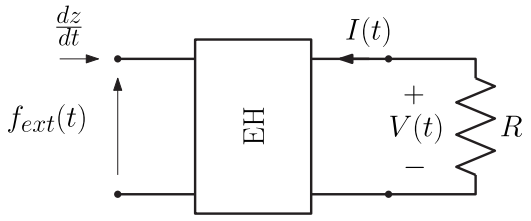

Fig. 4. Two-port network representation of a energy harvester for mechanical vibrations connected to a simple resistive load.

3.3. Stationary probability density function

Because the SDE (15) is single variable, the stationary probability density function (PDF) for the dimensionless energy $p_{st}(E)$ can be easily found solving the associated Fokker–Planck equation (FPE)

$$-\frac{\partial}{\partial E}\left(\overline{a}_E(E)p_{st}(E)\right)+\frac{1}{2}\frac{\partial^2}{\partial E^2}\left(\overline{B}_E^2(E)p_{st}(E)\right)=0 \tag{18}$$

Imposing null boundary conditions

$$\lim_{E\to+\infty} p_{st}(E)=\lim_{E\to+\infty}\frac{\partial p_{st}(E)}{\partial E}=0 \tag{19}$$

and by separation of variables, the following solution is found:

$$p_{st}(E)=\frac{\mathcal{N}}{\overline{B}_E^2(E)}\exp\left(2\int\frac{\overline{a}_E(E)}{\overline{B}_E^2(E)}dE\right) \tag{20}$$

where $\mathcal{N}$ is a constant whose value is determined imposing the normalization condition $\int_0^{+\infty} p_{st}(E)dE=1$.

For the angle variable, at the lowest order in ε, (13b) implies that the angle stationary PDF is found solving the FPE

$$-\Omega(E)\frac{\partial\hat{p}_{st}(\theta)}{\partial\theta}=0 \tag{21}$$

with periodic boundary condition. Imposing normalization yields $\hat{p}_{st}(\theta)=(2\pi)^{-1}$.

Since, after averaging and at the lowest order in ε, the energy and the angle are independent, the full stationary density function reads

$$P_{st}(E,\theta)=\hat{p}_{st}(\theta)\,p_{st}(E)=\frac{1}{2\pi}p_{st}(E) \tag{22}$$

Taking into account that the Jacobian of the coordinate change $(X_1,X_2)\to(E,\theta)$ is regular, the transformation can be inverted to find the explicit expressions for $X_1(E,\theta)$, and $X_2(E,\theta)$. From (8) we have

$$\mathbf{X}_e(E,\theta)=\mathbf{m}_1(E)X_1(E,\theta)+\mathbf{m}_2(E)X_2(E,\theta)$$

Therefore, the expectation of any arbitrary function $F(\mathbf{X}_e(E,\theta))$ can be evaluated as

$$E[F(\mathbf{X}_e(E,\theta))]=\frac{1}{2\pi}\int_0^{2\pi}\int_0^{+\infty}F(\mathbf{X}_e(E,\theta))\,p_{st}(E)\,dE\,d\theta \tag{23}$$

4. Piezoelectric harvester design

In this section, we apply the methodology developed above (Section 3), to the optimization of the cantilever beam, piezoelectric energy harvester described in Section 2. The cantilever beam is assumed to have a Duffing type nonlinearity, describing a stiffening effect of the beam, with elastic potential energy $U(Z_1)=(1/2)k_1\,Z_1^2+(1/4)k_3\,Z_1^4$, where k_1 and k_3 are constant parameters. The governing equations for the transducer are derived from the characterization of piezoelectric materials [46–48], obtaining

$$b_m(\mathbf{Z}_e)=-\alpha V \tag{24a}$$

$$C_{pz}\frac{dV}{dt}=\alpha Z_2+I \tag{24b}$$

where $\mathbf{Z}_e=[V,I]^T$ is the vector of the electrical variables (the transducer's output voltage and current), α is the electro-mechanical coupling constant (in N/V or As/m), and C_{pz} is the transducer's capacitance.

The final goal of an energy harvesting system is to supply power to a load, or possibly to recharge the load's internal battery. As a benchmark, first we consider the simple resistive load shown in Fig. 4. This is the most common setup considered in energy harvesting applications [13,17–19,42].

4.1. Resistive load

An electrical load is any two-terminal element that absorbs energy from the circuit. In energy harvesting applications, it is common to model the electrical load as a simple linear resistor, to keep the model mathematically tractable. However, in real applications, the electrical domain may include more complex two-terminal or two-port elements, possibly nonlinear, such as diode bridge rectifiers, exploited to transform the transducer output into a direct current.

From Ohm's law (passive sign convention), we have $I = -G\,V$, where $G = R^{-1}$ is the load conductance. The SDE system (3) becomes

$$dZ_1 = Z_2\,dt \tag{25a}$$

$$dZ_2 = \left(-\frac{1}{m}\hat{U}'(Z_1) - \frac{\hat{\varepsilon}}{m}Z_2 - \frac{\hat{\varepsilon}\alpha}{m}V\right)dt + \frac{\sqrt{\hat{\varepsilon}}}{m}dW_t \tag{25b}$$

$$dV = \frac{1}{C_{pz}}\left(\alpha Z_2 - G\,V\right)dt \tag{25c}$$

The dimensionless SDE system (6) is obtained from (25), using the normalizing diagonal matrix $\mathbf{P} = \mathrm{diag}[L_0^{-1}, T_0 L_0^{-1}, C_{pz}Q_0^{-1}]$, where L_0, Q_0 and T_0 are the normalizing length, charge and time, chosen as (values of L_0 and Q_0 are in magnitude):

$$L_0 = \frac{1}{\sqrt{k_1}}, \qquad Q_0 = \frac{C_{pz}}{\alpha\sqrt{m}}, \qquad T_0 = \sqrt{\frac{m}{k_1}} \tag{26}$$

The dimensionless SDE system reads

$$dX_1 = X_2\,dt \tag{27a}$$

$$dX_2 = \left(-X_1 - \kappa X_1^3 - \varepsilon X_2 - \varepsilon X_3\right)dt + \sqrt{\varepsilon}\,dW_t \tag{27b}$$

$$dX_3 = \left(\beta X_2 - \delta X_3\right)dt \tag{27c}$$

where $\mathbf{X}_t = [X_1, X_2, X_3]^T$ is the state vector whose components are the dimensionless displacement, velocity and output voltage, and the parameters are:

$$\kappa = \frac{k_3}{\sqrt{k_1}}, \qquad \varepsilon = \frac{\hat{\varepsilon}}{\sqrt{k_1\,m}},$$
$$\beta = \frac{\alpha^2}{C_{pz}}\sqrt{\frac{m}{k_1}}, \qquad \delta = \frac{G}{C_{pz}}\sqrt{\frac{m}{k_1}} \tag{28}$$

For $\varepsilon \to 0$ the solution of the SDEs (27a), (27b), approaches that of the underlying Hamiltonian system, which takes the form [29]:

$$X_1(E,\theta) = \left(\frac{4E^2}{1+4\kappa E}\right)^{1/4}\mathrm{sd}(\theta,k) \tag{29a}$$

$$X_2(E,\theta) = \sqrt{2E}\,\mathrm{cd}(\theta,k)\,\mathrm{nd}(\theta,k) \tag{29b}$$

where $E = X_2^2(0)/2 + U(X_1(0))$ is the value of the energy (determined by the initial conditions), $\mathrm{sd}(\theta,k)$, $\mathrm{cd}(\theta,k)$ and $\mathrm{nd}(\theta,k)$ are the Jacobi elliptic functions, and

$$k^2 = \frac{1}{2}\left(1 - \frac{1}{\sqrt{1+4\kappa E}}\right) \tag{30}$$

is the elliptic modulus [49]. The angle is $\theta(t) = \Omega(E)\,t$, with angular frequency

$$\Omega(E) = (1+4\kappa E)^{1/4} \tag{31}$$

A straightforward application of Lemma 1 yields

$$m_1(E) = \frac{\beta\,\Omega^2(E)}{\delta^2 + \Omega^2(E)} \tag{32a}$$

$$m_2(E) = \frac{\delta\,\beta}{\delta^2 + \Omega^2(E)} \tag{32b}$$

Substituting (8) into (27) results into the reduced order model

$$dX_1 = X_2\,dt \tag{33a}$$

$$dX_2 = \left(-(1+\varepsilon m_1)X_1 - \kappa X_1^3 - \varepsilon(1+m_2)X_2\right)dt + \sqrt{\varepsilon}\,dW_t \tag{33b}$$

We stress again that, as the energy is nearly constant, m_1 and m_2 are constant as well. Therefore, the explicit dependence of the coefficient on E is omitted for clarity of notation.

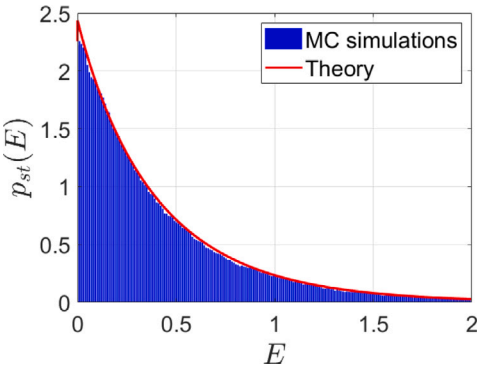

Fig. 5. Stationary probability density function for the dimensionless energy of the SDEs system (27). Parameters values are: $\kappa = 1$, $\beta = 0.5$, $\delta = 50$, and $\varepsilon = 0.25$.

The coefficients of the averaged energy equation take the form

$$\overline{a}_E(E) = \frac{1}{2\pi}\int_0^{2\pi}\left(\frac{1}{2} - (1+m_2)X_2^2(E,\theta) - m_1 X_1(E,\theta)X_2(E,\theta)\right)d\theta \tag{34a}$$

$$\overline{B}_E(E) = \left(\frac{1}{2\pi}\int_0^{2\pi} X_2^2(E,\theta)d\theta\right)^{\frac{1}{2}} \tag{34b}$$

Using the results in Appendix, the following expressions for the averaged coefficients are found

$$\overline{a}_E(E) = \frac{1}{2} - \frac{1+m_2(E)}{2\,k^2\,\mathcal{K}(k)}E\left(I_2 - k'^2 I_4\right) \tag{35a}$$

$$\overline{B}_E(E) = \left(\frac{E}{2\,k^2\,\mathcal{K}(k)}\left(I_2 - k'^2 I_4\right)\right)^{\frac{1}{2}} \tag{35b}$$

where $\mathcal{K}(k)$ is the complete elliptic integral of the first kind and k' is the complementary modulus. The coefficients $\overline{a}_E(E)$ and $\overline{B}_E(E)$ are finally used to calculate the stationary marginal PDF for the energy, according to (20).

The stationary marginal PDF for the energy calculated above, is compared against numerical result in Fig. 5, demonstrating the accuracy of the approximations used in the derivation. The numerical marginal PDF is calculated through Monte-Carlo simulations, integrating numerically the SDE system (27), using the stochastic Runge–Kutta of strong order 1 method [38,50]. The time integration length was $\Delta T = 10^4$ (dimensionless time), resulting in a normalized time integration step ($\delta t \simeq 37 \times 10^{-6}$). Results were obtained averaging over 20 simulations carried out for different realizations of the Wiener process, removing the initial transient interval $\Delta\tau$ from the data for each simulation. Because the realizations of the Wiener processes are independent, the resulting data is equivalent to a longer $(20(\Delta T - \Delta\tau))$ time simulation. The probability to find the system in each energy interval $(E, E + dE)$, is defined as the number of samples in that interval, divided by the total number of samples.

As a figure of merit for the harvester's performance, we use the dimensionless root mean square output voltage $X_{3,(rms)} = \sqrt{\mathrm{E}[X_3^2]}$. According to (8), the expectation $E[X_3^2]$ is given by

$$\mathrm{E}[X_3^2] = \frac{1}{2\pi}\int_0^{2\pi}\int_0^{+\infty}\left(m_1(E)X_1(E,\theta) + m_2 X_2(E,\theta)\right)^2 p_{st}(E)\,dE\,d\theta \tag{36}$$

The integration with respect to the angle is discussed in Appendix, whereas the integration with respect to the energy is carried out numerically. Fig. 6 shows the dimensionless root mean square output voltage $X_{3,(rms)}$ versus parameter δ. Blue squares are expectations determined from numerical simulations, while the red line is the theoretical prediction obtained with the proposed method. Again, agreement is excellent, thus validating the proposed approach.

4.2. Matched load

Inspired by our recent works [26,30,31], as a second example we consider the piezoelectric energy harvester with a matched electrical load shown in Fig. 7. The reactive behavior of the piezoelectric transducer implies that part of the injected energy is stored, and later reflected to the source, by the transducer. Such a reactive power cannot be converted into useful average power, thus significantly reducing the harvested power and the power efficiency. The role of the matching network is to reduce this reactive energy, often interpreted as a mismatch between the electrical and the mechanical parts of the harvester. Obviously, perfect matching is possible only at a specific frequency. Nonetheless, a proper design of the matching network allows to achieve a partial matching over a relatively wide frequency interval, thus increasing significantly the output voltage and the harvested power delivered to the load.

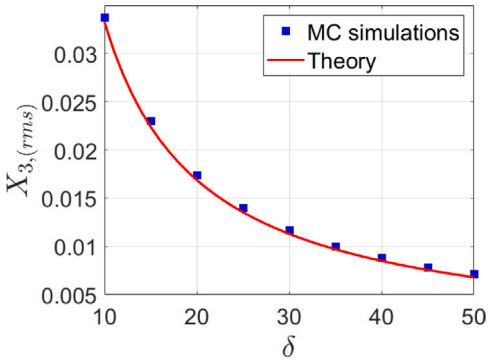

Fig. 6. Dimensionless root mean square output voltage $X_{3,(rms)}$ versus parameter δ, for the energy harvester with resistive load. Other parameters values are: $\kappa = 1$, $\beta = 0.5$, and $\varepsilon = 0.25$.

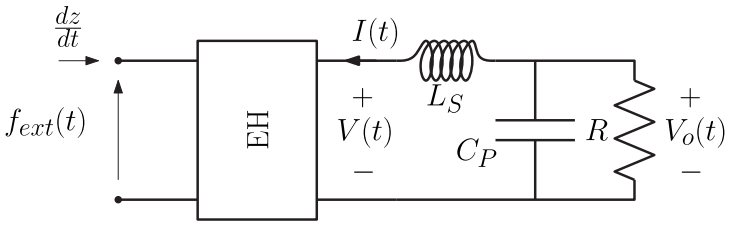

Fig. 7. Two-port network representation of a energy harvester for mechanical vibrations, with a low-pass L-matching network interposed between the harvester and the resistive load.

Taking into account the harvester nonlinearity prevents an analytical determination of the optimal reactance values of the electrical components in the matching network. Their optimal value with respect to a prescribed metric can be found numerically, but the calculation requires lengthy simulations, an approach that becomes unfeasible if a large parameter space must be explored. By contrast, applying the method proposed in this work, most of the calculations can be carried out analytically, with only the PDF and the output voltage requiring numerical integration steps, a task that can be performed in few seconds.

Considering the circuit shown in Fig. 7, application of Kirchhoff laws gives the governing equations

$$dZ_1 = Z_2\,dt \tag{37a}$$

$$dZ_2 = \left(-\frac{1}{m}\hat{U}'(Z_1) - \frac{\hat{\varepsilon}}{m}Z_2 - \frac{\hat{\varepsilon}\alpha}{m}V\right)dt + \frac{\sqrt{\hat{\varepsilon}}}{m}dW_t \tag{37b}$$

$$dV = \frac{1}{C_{pz}}(\alpha Z_2 - I)dt \tag{37c}$$

$$dI = \frac{1}{L_S}(V - V_o)dt \tag{37d}$$

$$dV_o = \frac{1}{C_P}(I - G\,V_o)dt \tag{37e}$$

where V_o is the output voltage, and L_S and C_P are the inductance and capacitance parameters of the matching network that should be optimized.

Introducing the diagonal matrix

$$\mathbf{P} = \mathrm{diag}[L_0^{-1}, T_0 L_0^{-1}, C_{pz}Q_0^{-1}, T_0 Q_0^{-1}, C_{pz}Q_0^{-1}]$$

where L_0, Q_0 and T_0 are defined in (25), the following normalized SDE system is obtained

$$dX_1 = X_2\,dt \tag{38a}$$

$$dX_2 = \left(-X_1 - \kappa X_1^3 - \varepsilon X_2 - \varepsilon X_3\right)dt + \sqrt{\varepsilon}\,dW_t \tag{38b}$$

$$dX_3 = \left(\beta X_2 - X_4\right)dt \tag{38c}$$

$$dX_4 = \mu\left(X_3 - X_5\right)dt \tag{38d}$$

$$dX_5 = \left(\nu X_4 - \hat{\delta}X_5\right)dt \tag{38e}$$

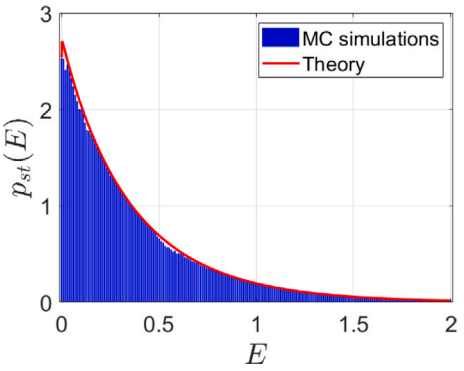

Fig. 8. Stationary probability density function for the dimensionless energy of the SDEs system (38). Parameters values are: $\kappa = 1$, $\beta = 0.5$, $\hat{\delta} = 50$, $\mu = \nu = 10$, and $\varepsilon = 0.25$.

where $\mathbf{X}_t = [X_1, \dots, X_5]^T$ is the state vector which components are the (dimensionless) displacement, velocity, voltage across the transducer, output current and output voltage, respectively. The values of coefficients κ, ε and β follow (28), and

$$\mu = \frac{m}{C_{pz}\, L_S\, k_1}, \qquad \nu = \frac{C_{pz}}{C_P}, \qquad \hat{\delta} = \frac{G}{C_P}\sqrt{\frac{m}{k_1}} \tag{39}$$

Defining the complex quantities

$$S = \beta \frac{1 + j\Omega \dfrac{j\Omega + \hat{\delta}}{\mu\nu}}{j\Omega - \Omega^2 \dfrac{j\Omega + \hat{\delta}}{\mu\nu} + \dfrac{j\Omega + \hat{\delta}}{\nu}} \tag{40a}$$

$$T = \beta \left(j\Omega - \Omega^2 \frac{j\Omega + \hat{\delta}}{\mu\nu} + \frac{j\Omega + \hat{\delta}}{\nu} \right)^{-1} \tag{40b}$$

and using Lemma 1, we find

$$m_{1,1} = -\Omega \,\mathrm{Im}\,\{S\} \tag{41a}$$

$$m_{2,1} = \mathrm{Re}\,\{S\} \tag{41b}$$

$$m_{1,3} = -\Omega \,\mathrm{Im}\,\{T\} \tag{41c}$$

$$m_{2,3} = \mathrm{Re}\,\{T\} \tag{41d}$$

where $m_{i,j}(E)$ denotes the jth component of vector $\mathbf{m}_i$.

The reduced order model and the coefficients of the averaged equations are identical to (33) and (35), respectively, with m_1 and m_2 replaced by $m_{1,1}$ and $m_{2,1}$. Fig. 8 shows a comparison between the stationary marginal PDF computed from numerical simulations and the theoretical prediction.

For the rms output voltage, we calculate the expectation $\mathrm{E}[X_5^2]$, thereby obtaining:

$$\mathrm{E}[X_5^2] = \frac{1}{2\pi} \int_0^{2\pi} \int_0^{+\infty} \left(m_{1,3}(E) X_1(E,\theta) + m_{2,3} X_2(E,\theta) \right)^2 p_{st}(E)\, dE\, d\theta \tag{42}$$

As in the previous example, integration with respect to the angle is described in Appendix, while integration with respect to energy is calculated numerically.

Fig. 9 shows the dimensionless root mean square output voltage $X_{5,(rms)}$ versus the parameter $\hat{\delta}$, for two different set of values of the parameters μ, ν, that are associated to the capacitance and inductance of the electrical elements in the matching network. Blue and black squares are numerical results obtained from Monte-Carlo simulations, while red lines correspond to the proposed approach. Blue squares and solid red line are results for $\mu = \nu = 10$, while black squares and dashed red line are for $\mu = \nu = 100$.

Finally, Fig. 10 shows $X_{5,(rms)} = \sqrt{\mathrm{E}[X_5^2]}$ versus parameters μ and ν. The relationship between μ, ν, and L_S, C_P is defined in (39). Calculating the dimensionless output voltage for different values of μ and ν, it is possible to determine the parameters' values that maximize the output voltage, thus optimizing the matching network. In particular, we have calculated the output voltages for $\mu \in (0, 5]$, and $\nu \in [1, 50]$. We found that the output voltage has a maximum of $X_{5,(rms)} = 0.2657$ at $\mu_{opt} = 1.05$, $\nu_{opt} = 50$. It is worth noticing that the output voltage is strictly increasing for increasing values of μ, with a saturating effect. As a last remark, we observe that exploiting the matching network increases the maximum output voltage by a factor of about 8, with respect to the energy harvester with a simple, unmatched resistive load.

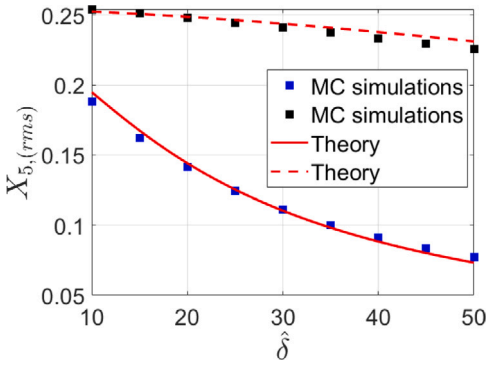

Fig. 9. Dimensionless root mean square output voltage $X_{5,(rms)}$, versus parameter $\hat{\delta}$, for the energy harvester with matched load. Blue squares: Monte-Carlo simulations for $\mu = \nu = 10$. Black squares: Monte-Carlo simulations for $\mu = \nu = 100$. Red lines are theoretical predictions. Other parameters values are: $\kappa = 1$, $\beta = 0.5$, and $\varepsilon = 0.25$.

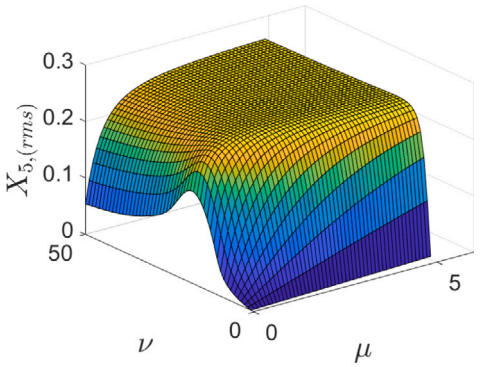

Fig. 10. Dimensionless output voltage root mean square $X_{5,(rms)}$ versus parameters μ and ν, for the energy harvester with matched load. Other parameters values are: $\kappa = 1$, $\beta = 0.5$, $\hat{\delta} = 10$, and $\varepsilon = 0.25$.

5. Conclusions

This paper presented a methodology for the analysis, design, and optimization of electro-mechanical systems for energy harvesting applications. The method is based on model order reduction and stochastic averaging, and it is suitable for application to nonlinear energy harvesters for ambient mechanical vibrations modeled as white Gaussian noise.

The procedure permits the reduction of the system of nonlinear stochastic differential equations describing the harvester, to a single stochastic equation for the mechanical energy. The simplified system was then solved, obtaining the relevant expected quantities like average harvested power and the root mean square output voltage. In particular, the simplified model made the calculation of expected quantities relatively easy, allowing for the exploration of a large parameter space. In contrast, traditional approaches would require lengthy, time-consuming Monte Carlo simulations.

As an example, the method was applied to the analysis of a nonlinear, piezoelectric energy harvester with two different load setups: a simple resistive load, and a matched load. The method was validated against Monte Carlo simulations, providing a numerical solution of the original, nonlinear stochastic model. The method shows good accuracy, and it proves effective in reducing computational complexity providing a simple and efficient tool for the design of the matching network.

Finally, the energy harvester with a matched load was shown to offer a significant boost in terms of root mean square output voltage with respect to a simple, non-matched load.

CRediT authorship contribution statement

Kailing Song: Writing – review & editing, Visualization, Validation, Software, Resources, Methodology, Investigation, Formal analysis, Data curation, Conceptualization. **Michele Bonnin:** Writing – review & editing, Writing – original draft, Visualization, Validation, Supervision, Software, Resources, Project administration, Methodology, Investigation, Funding acquisition, Formal analysis, Data curation, Conceptualization. **Fabio L. Traversa:** Writing – review & editing, Validation, Investigation, Formal analysis, Conceptualization. **Fabrizio Bonani:** Writing – review & editing, Supervision, Resources, Methodology, Investigation, Formal analysis, Conceptualization.

Declaration of competing interest

The authors declare that they have no known competing financial interests or personal relationships that could have appeared to influence the work reported in this paper.

Data availability

Data will be made available on request.

Acknowledgments

This research has been partially conducted within the Italian inter-university PhD course in Sustainable Development and Climate Change.

Appendix. Integrals of powers of the Jacobi elliptic functions

The calculation of the averaged coefficients (34) and of the root mean square output voltages (36), (42) require to evaluate the integrals

$$\frac{1}{2\pi}\int_0^{2\pi} X_1^2(E,\theta)\,d\theta = \frac{2E}{\sqrt{1+4\kappa E}}\int_0^{4\mathcal{K}(k)} \mathrm{sd}^2(u)\,du \tag{A.1}$$

$$\frac{1}{2\pi}\int_0^{2\pi} X_1(E,\theta)X_2(E,\theta)\,d\theta = \frac{2E}{(1+4\kappa E)^{1/4}}\int_0^{4\mathcal{K}(k)} \mathrm{sd}(u)\,\mathrm{cd}(u)\,\mathrm{nd}(u)\,du \tag{A.2}$$

$$\frac{1}{2\pi}\int_0^{2\pi} X_2^2(E,\theta)\,d\theta = 2E\int_0^{4\mathcal{K}(k)} \mathrm{cd}^2(u)\,\mathrm{nd}^2(u) \tag{A.3}$$

Integrals (A.1) and (A.3) can be evaluated using the relationships between the squares of the Jacobi elliptic functions:

$$k^2\mathrm{sd}^2(u) = \mathrm{nd}^2(u) - 1 \tag{A.4}$$

$$k^2\mathrm{cd}^2(u) = 1 - k'^2\mathrm{nd}^2(u) \tag{A.5}$$

where $k'^2 = 1-k^2$ is the complementary modulus. Substituting into (A.1) and (A.3), integrals of the following kind must be evaluated for even n

$$I_n = \int_0^{4\mathcal{K}(k)} \mathrm{nd}^n(u)\,du \tag{A.6}$$

Lemma 3. *Integral (A.6) admits the following recursive solution:*

$$I_2 = \frac{4\mathcal{E}(k)}{k'^2} \tag{A.7}$$

$$I_4 = \frac{8(2-k'^2)\mathcal{E}(k) - 4(1-k^2)\mathcal{K}(k)}{3k'^4} \tag{A.8}$$

$$I_n = \frac{1}{(1-n)k'^2}\left((2-n)(k'^2+1)I_{n-2} + (n-3)I_{n-4}\right), \quad n = 6, 8, \ldots \tag{A.9}$$

where $\mathcal{K}(k)$ and $\mathcal{E}(k)$ are the complete elliptic integrals of the first and second kind, respectively [49].

Proof. For $n = 2, 4$, integral (A.6) is solved using the Fourier series for $\mathrm{nd}^2(u)$, and $\mathrm{nd}^4(u)$ [51]:

$$\mathrm{nd}^2(u) = \frac{\mathcal{E}(k)}{k'^2\,\mathcal{K}(k)} + \frac{\pi^2}{k'^2\,\mathcal{K}^2(k)}\sum_{n=1}^{+\infty}(-1)^n n\,\mathrm{csch}(2nW_0)\cos\left(\frac{n\pi u}{\mathcal{K}(k)}\right) \tag{A.10}$$

$$\mathrm{nd}^4(u) = \frac{2(2-k^2)\mathcal{E}(k) - (1-k^2)\mathcal{K}(k)}{3k'^4\mathcal{K}(k)} + \frac{\pi^2}{6k'^4\,\mathcal{K}(k)}\sum_{n=1}^{+\infty}(-1)^n n\left(\left(\frac{n\pi}{\mathcal{K}(k)}\right)^2 + 4(2-k^2)\right)\mathrm{csch}(2nW_0)\cos\left(\frac{n\pi u}{\mathcal{K}(k)}\right) \tag{A.11}$$

where

$$W_0 = \frac{\pi\mathcal{K}(k')}{2\mathcal{K}(k)} \tag{A.12}$$

For larger, even values of n, we proceed as follows: we consider first the differential relationships of Jacobi elliptic functions, enabling to obtain

$$\frac{d}{du}\left[\mathrm{nd}^m(u)\,\mathrm{sd}(u)\,\mathrm{cd}(u)\right] = -(m+2)\frac{k'^2}{k^2}\,\mathrm{nd}^{m+3}(u) + (m+1)\frac{k'^2+1}{k^2}\,\mathrm{nd}^{m+1}(u) - m\frac{1}{k^2}\,\mathrm{nd}^{m-1}(u) \tag{A.13}$$

For $m = n - 3$

$$\frac{d}{du}\left[\mathrm{nd}^{n-3}(u)\,\mathrm{sd}(u)\,\mathrm{cd}(u)\right] = (1-n)\frac{k'^2}{k^2}\,\mathrm{nd}^{n}(u) + (n-2)\frac{k'^2+1}{k^2}\,\mathrm{nd}^{n-2}(u) - (n-3)\frac{1}{k^2}\,\mathrm{nd}^{n-4}(u) \tag{A.14}$$

After integration, taking into account that the integral on the left hand side is null, and rearranging the terms we obtain (A.9). □

We obtain

$$\frac{1}{2\pi}\int_0^{2\pi} X_2^2(E,\theta)\,d\theta = \frac{E}{2\,k^2\,\mathcal{K}(k)}\left(I_2 - k'^2 I_4\right) \tag{A.15}$$

$$\frac{1}{2\pi}\int_0^{2\pi} X_1^2(E,\theta)\,d\theta = \frac{1}{4\,k^2\,\mathcal{K}(k)}\frac{2E}{\sqrt{1+4\kappa E}}\left(I_2 - 4\mathcal{K}(k)\right) \tag{A.16}$$

Finally, integral (A.2) is null because of the periodicity of Jacobi elliptic functions.

References

[1] Misra S, Mukherjee A, Roy A. Introduction to IoT. Cambridge University Press; 2021.
[2] Penella-López MT, Gasulla-Forner M. Powering autonomous sensors an integral approach with focus on solar and RF energy harvesting. Springer; 2011.
[3] Roundy S, Wright PK, Rabaey JM. Energy scavenging for wireless sensor networks. Springer; 2003.
[4] Paradiso JA, Starner T. Energy scavenging for mobile and wireless electronics. IEEE Pervasive Comput 2005;4(1):18–27. http://dx.doi.org/10.1109/MPRV.2005.9.
[5] Beeby SP, Tudor MJ, White NM. Energy harvesting vibration sources for microsystems applications. Meas Sci Technol 2006;17(12):R175. http://dx.doi.org/10.1088/0957-0233/17/12/R01.
[6] Mitcheson P, Yeatman E, Rao G, Holmes A, Green T. Energy harvesting from human and machine motion for wireless electronic devices. Proc IEEE 2008;96(9):1457–86. http://dx.doi.org/10.1109/jproc.2008.927494.
[7] Lu X, Wang P, Niyato D, Kim DI, Han Z. Wireless networks with RF energy harvesting: A contemporary survey. IEEE Commun Surv Tutor 2015;17(2):757–89. http://dx.doi.org/10.1109/comst.2014.2368999.
[8] Akinaga H. Recent advances and future prospects in energy harvesting technologies. Japan J Appl Phys 2020;59(11):110201. http://dx.doi.org/10.35848/1347-4065/abbfa0.
[9] Clemente CS, Davino D, Loschiavo VP. Analysis of a magnetostrictive harvester with a fully coupled nonlinear FEM modeling. IEEE Trans Magn 2021;57(6):1–4. http://dx.doi.org/10.1109/TMAG.2021.3059927.
[10] Li T, Lee PS. Piezoelectric energy harvesting technology: From materials, structures, to applications. Small Struct 2022;3(3). http://dx.doi.org/10.1002/sstr.202100128.
[11] Kim H, Priya S, Stephanou H, Uchino K. Consideration of impedance matching techniques for efficient piezoelectric energy harvesting. IEEE Trans Ultrason Ferroelectr Freq Control 2007;54(9):1851–9. http://dx.doi.org/10.1109/tuffc.2007.469.
[12] Roscow JI, Pearce H, Khanbareh H, Kar-Narayan S, Bowen CR. Modified energy harvesting figures of merit for stress- and strain-driven piezoelectric systems. Eur Phys J Spec Top 2019;228(7):1537–54. http://dx.doi.org/10.1140/epjst/e2019-800143-7.
[13] Kurt P, Narayan B, Roscow JI, Orhan S. Improving piezoelectric energy harvesting performance through mechanical stiffness matching. Mech Adv Mater Struct 2023;1–14. http://dx.doi.org/10.1080/15376494.2023.2295383.
[14] Roundy S, Zhang Y. Toward self-tuning adaptive vibration-based microgenerators. In: Smart structures, devices, and systems II, vol. 5649. SPIE; 2005, p. 373–84. http://dx.doi.org/10.1117/12.581887.
[15] Roundy S. On the effectiveness of vibration-based energy harvesting. J Intell Mater Syst Struct 2005;16(10):809–23. http://dx.doi.org/10.1177/1045389X05054042.
[16] Blokhina E, El Aroudi A, Alarcon E, Galayko D. Nonlinearity in energy harvesting systems. Micro- and Nanoscale Applications. Springer; 2016.
[17] Rosso M, Nastro A, Baù M, Ferrari M, Ferrari V, Corigliano A, Ardito R. Piezoelectric energy harvesting from low-frequency vibrations based on magnetic plucking and indirect impacts. Sensors 2022;22(15):5911. http://dx.doi.org/10.3390/s22155911.
[18] Cottone F, Vocca H, Gammaitoni L. Nonlinear energy harvesting. Phys Rev Lett 2009;102(8):080601. http://dx.doi.org/10.1103/PhysRevLett.102.080601.
[19] Stanton SC, McGehee CC, Mann BP. Reversible hysteresis for broadband magnetopiezoelastic energy harvesting. Appl Phys Lett 2009;95(17). http://dx.doi.org/10.1063/1.3253710.
[20] Hajati A, Kim S-G. Ultra-wide bandwidth piezoelectric energy harvesting. Appl Phys Lett 2011;99(8):083105. http://dx.doi.org/10.1063/1.3629551.
[21] Arrieta A, Hagedorn P, Erturk A, Inman DJ. A piezoelectric bistable plate for nonlinear broadband energy harvesting. Appl Phys Lett 2010;97(10):104102. http://dx.doi.org/10.1063/1.3487780.
[22] Cottone F, Basset P, Vocca H, Gammaitoni L, Bourouina T. Bistable electromagnetic generator based on buckled beams for vibration energy harvesting. J Intell Mater Syst Struct 2014;25(12):1484–95. http://dx.doi.org/10.1177/1045389X13508330.
[23] Zhou S, Lallart M, Erturk A. Multistable vibration energy harvesters: Principle, progress, and perspectives. J Sound Vib 2022;528:116886. http://dx.doi.org/10.1016/j.jsv.2022.116886.
[24] Rosso M, Ardito R. A review of nonlinear mechanisms for frequency up-conversion in energy harvesting. Actuators 2023;12(12). http://dx.doi.org/10.3390/act12120456.
[25] Rosso M, Cuccurullo S, Perli FP, Maspero F, Corigliano A, Ardito R. A method to enhance the nonlinear magnetic plucking for vibration energy harvesters. 2023, http://dx.doi.org/10.21203/rs.3.rs-3331471/v1.
[26] Song K, Bonnin M, Traversa FL, Bonani F. Stochastic analysis of a bistable piezoelectric energy harvester with a matched electrical load. Nonlinear Dynam 2023;111(18):16991–7005. http://dx.doi.org/10.1007/s11071-023-08746-7.
[27] Yan Z, Sun W, Hajj MR, Zhang W, Tan T. Ultra-broadband piezoelectric energy harvesting via bistable multi-hardening and multi-softening. Nonlinear Dynam 2020;100:1057–77. http://dx.doi.org/10.1007/s11071-020-05594-7.
[28] Yu T, Zhou S. Performance investigations of nonlinear piezoelectric energy harvesters with a resonant circuit under white Gaussian noises. Nonlinear Dynam 2021;103(1):183–96. http://dx.doi.org/10.1007/s11071-020-06170-9.
[29] Bonnin M, Traversa FL, Bonani F. Leveraging circuit theory and nonlinear dynamics for the efficiency improvement of energy harvesting. Nonlinear Dynam 2021;104(1):367–82. http://dx.doi.org/10.1007/s11071-021-06297-3.
[30] Bonnin M, Traversa FL, Bonani F. An impedance matching solution to increase the harvested power and efficiency of nonlinear piezoelectric energy harvesters. Energies 2022;15(8):2764. http://dx.doi.org/10.3390/en15082764.
[31] Bonnin M, Song K. Frequency domain analysis of a piezoelectric energy harvester with impedance matching network. Energy Harvest Syst 2022;10(1):119–33. http://dx.doi.org/10.1515/ehs-2022-0077.

[32] Di Monaco F, Tehrani MG, Elliott SJ, Bonisoli E, Tornincasa S. Energy harvesting using semi-active control. J Sound Vib 2013;332(23):6033–43. http://dx.doi.org/10.1016/j.jsv.2013.06.005.
[33] Caruso G, Galeani S, Menini L. Semi-active damping and energy harvesting using an electromagnetic transducer. J Vib Control 2018;24(12):2542–61. http://dx.doi.org/10.1177/1077546316688993.
[34] Costanzo L, Lo Schiavo A, Vitelli M. A self-supplied power optimizer for piezoelectric energy harvesters operating under non-sinusoidal vibrations. Energies 2023;16(11):4368. http://dx.doi.org/10.3390/en16114368.
[35] Covaci C, Gontean A. Piezoelectric energy harvesting solutions: A review. Sensors 2020;20(12):3512. http://dx.doi.org/10.3390/s20123512.
[36] Sezer N, Koç M. A comprehensive review on the state-of-the-art of piezoelectric energy harvesting. Nano Energy 2021;80:105567. http://dx.doi.org/10.1016/j.nanoen.2020.105567.
[37] Chua LO, Desoer CA, Kuh ES. Linear and nonlinear circuits. McGraw-Hill; 1987.
[38] Bonnin M, Song K, Traversa FL, Bonani F. A circuit theory perspective on the modeling and analysis of vibration energy harvesting systems: A review. Computation 2023;11(3):45. http://dx.doi.org/10.3390/computation11030045.
[39] Øksendal B. Stochastic differential equations. 6th ed.. Springer; 2003.
[40] Bonnin M, Song K, Traversa FL, Bonani F. Model order reduction and stochastic averaging for the analysis and design of micro-electro-mechanical systems. Nonlinear Dynam 2024;112. http://dx.doi.org/10.1007/s11071-023-09225-9.
[41] Schilders WH, Vorst HA, Rommes J. Model order reduction: Theory, research aspects and applications. Springer; 2008.
[42] Xu M, Jin X, Wang Y, Huang Z. Stochastic averaging for nonlinear vibration energy harvesting system. Nonlinear Dynam 2014;78(2):1451–9. http://dx.doi.org/10.1007/s11071-014-1527-6.
[43] Goldstein H, Poole C, Safko J. Classical mechanics. Pearson; 2001.
[44] Khasminskii R. On the principle of averaging the Ito's stochastic differential equations. Kibernetika 1968;4(3):260–79.
[45] Bonnin M, Traversa FL, Bonani F. Analysis of influence of nonlinearities and noise correlation time in a single-DOF energy-harvesting system via power balance description. Nonlinear Dynam 2020;100(1):119–33. http://dx.doi.org/10.1007/s11071-020-05563-0.
[46] Jones TB, Nenadic NG. Electromechanics and MEMS. Cambridge University Press; 2013.
[47] Priya S, Inman DJ. Energy harvesting technologies. Springer; 2009, p. 517.
[48] IEEE standard on piezoelectricity. 1988, http://dx.doi.org/10.1109/ieeestd.1988.79638.
[49] Byrd PF, Friedman MD. Handbook of elliptic integrals for engineers and physicists. Springer; 2013.
[50] Särkkä S, Solin A. Applied stochastic differential equations. Cambridge University Press; 2019.
[51] Shi-Dong W, Ji-Bin L. Fourier series of rational fractions of Jacobian elliptic functions. Appl Math Mech 1988;9(6):541–56. http://dx.doi.org/10.1007/BF02465410.